Corrosion Science 138 (2018) 275–283

Contents lists available at ScienceDirect

Corrosion Science

journal homepage: www.elsevier.com/locate/corsci

Severe corrosion of steel and copper by strontium bromide in thermochemical heat storage reactors

Pierre D'Ans[a,*], Emilie Courbon[b], Marc Frère[b], Gilbert Descy[c], Tiriana Segato[a], Marc Degrez[a]

[a] Université Libre de Bruxelles (ULB), 4MAT Department, 50, Avenue F.D. Roosevelt, CP194/03, 1050, Brussels, Belgium
[b] UMONS, Institut de Recherche en Energie – Laboratoire de Thermodynamique, 31 Boulevard Dolez, 7000, Mons, Belgium
[c] BE-SOL R&D, 2 rue de la Griotte, 5580, Rochefort, Belgium

ARTICLE INFO

Keywords:
A. Copper
A. Carbon steel
B. Weight loss
B. XRD
B. Cyclic voltammetry
C. Reactor conditions

ABSTRACT

Thermochemical heat storage exploits thermal solar energy to produce sustainable residential heating, obtained by exothermal reaction between bromides and water vapour. A protocol to test the corrosion of surrounding materials is discussed in the case of $SrBr_2$ contacting copper or steel. Corrosion depth > 1 mm y^{-1} is found for steel in conditions where the salt remains mostly solid, due to a reaction between $SrBr_2$ and atmospheric CO_2 that produces HBr. Temperature and the dissolution of the salt (deliquescence) also play a key role. Potentiodynamic tests, the limitations of which are discussed, corroborate the salt degradation in the case of steel.

1. Introduction

While electrical power storage is becoming widespread through applications like electrical vehicles, thermal energy storage still needs some developments to be available at large scale. A targeted application is residential space heating, which would make it possible to store low grade heat (< 100 °C) that cannot be easily valorised for other applications (e.g. industrial waste heat and heat from thermal solar collectors). In order to tend towards seasonal heat storage, technologies like sensible heat storage, latent heat storage (using phase change materials, PCMs) and thermochemical heat storage were developed [1]. In the latter case, the technology can exploit the exothermal hydration of a hygroscopic salt in wintertime, which is dehydrated again in summertime, by connecting the salt container to a cheap source of heat. Other sorbents than water can be used as well. Hydrates of $MgSO_4$ [2], $MgCl_2$ [3], $SrBr_2$ [4–6], $CaCl_2$ [7–9], LiBr [10], Na_2S [11] and cementitious materials [12] make it possible to reach energy densities up to several hundreds of kWh/m^3 [13]. Physical sorbents and composite sorbents, generally made of salt encapsulated in a matrix, are also promising [14–20].

Running these systems implies designing a chemical reactor with surfaces that support the active material and are exposed to high moisture atmosphere, above room temperature. In an open system, the materials are exposed to air from outside the reactor as well, which is the case in the present paper. At a first glance, this situation is prone to generate corrosion of the reactor.

Since the late eighties, several papers have been dedicated to the corrosion problem in the case of PCMs, with tests focused on the melting process or the liquid phase [21–34], and quite often in organic compounds [30,35,36]. In the case of thermochemical storage, Simonova et al. briefly justified the encapsulation of salts in inert matrices by several factors like their corrosiveness [37]. The descriptions in some patents on heat storage systems contain information on the materials used, but without any corrosion data. In a system based on the adsorption of ammonia onto $CaCl_2$ or $BaCl_2$, Coldway s.a. uses stainless steel [38]. French *Commissariat à l'Energie Atomique* suggests using stainless steel, hard chrome plating or aluminium for components in contact with pure strontium bromide. More specifically, Solé et al. tested a selection of metals in the presence of several salts. In the conditions of their tests, they recommend, for instance, stainless steel in the presence of $CaCl_2$ [39,40]. However, the testing atmosphere is nearly saturated in water [39,40] and the salts attract molecules of water contained in the ambient atmosphere until dissolution. This phenomenon is sometimes referred to as deliquescence. The same author reported on the corrosiveness of Na_2S hydrates for copper and recommended the use of coatings to protect metal in the presence of this salt [11].

Present work is dedicated to a thermochemical storage using mono- and hexahydrate $SrBr_2$. No recommendation for the selection of materials is given in the literature regarding $SrBr_2$; more data is available regarding the storage of liquid Br_2 [41] and the selection of materials in contact with it [42–45], as well as in bromide solutions [46].

* Corresponding author.
E-mail address: pdans@ulb.ac.be (P. D'Ans).

https://doi.org/10.1016/j.corsci.2018.04.020
Received 11 October 2016; Received in revised form 10 April 2018; Accepted 11 April 2018
Available online 17 April 2018
0010-938X/

Like other salts, $SrBr_2$ is prone to dissolution and a curve can be drawn in the (temperature, partial pressure of water) plan, to delimit the domains of "solid" strontium bromide (with hydration water), and "dissolved" strontium bromide [47]. Accidental dissolution not only degrades the properties of the solid salt, but is also a possible factor of corrosion.

A reduced amount of papers deals with the corrosion at quite low temperature of at least partially solid salts in contact with metals. A quite similar problem was studied in the work of Badwe et al., where brines were progressively dried, in contact with metal, used for the storage of nuclear waste [48]. In the case of moist $MgCl_2$, corrosion was studied yet by bringing water using another salt [49]. Another testing strategy is to insert samples of metals in contact with the salt in a climatic chamber that is able to control moisture. Such a device is normally designed to study the atmospheric corrosion, but it is also useful for the corrosion in a particle-containing atmosphere [50]. One of the previously mentioned works is also based on such a system, but, again, in liquid conditions [39].

In this paper, a similar testing procedure is proposed, for both sides of the dissolution line. The behavior of low carbon steel and copper is described in the presence of strontium bromide, in various conditions that are likely to be encountered in a thermochemical reactor for space heating application. These materials are studied because they were candidates for a prototype developed in a wider project, SOLAUTARK, where seasonal heating is experienced. Operational conditions include temperatures in the 30–80 °C range and nominal partial pressure of water of 1250 Pa, with important local differences. In operation, both copper and steel suffered from severe corrosion, even in occasional contact with $SrBr_2$. Then, the paper tries to answer the following questions:

(i) How severe is the corrosion in these conditions?
(ii) If relevant, how the operating conditions do influence the phenomenon?
(iii) What is the corrosion mechanism?

2. Materials and methods

Tested materials consist of sections of St37 steel bar (diameter ~10 mm, height ~10 mm) and plates of copper (commercial purity) (~10 mm × 10 mm). Traces of oxidations are removed prior to experiments. Exact dimensions are measured for each sample using a Vernier scale, so as to determine the exposed surface area.

Strontium bromide hexahydrate (99%, Alfa Aesar) is manually crushed prior to experiments and is used as a corrosive medium.

Experiments are based on mass change during corrosion test and visual inspection of corrosion products. Coupons of the studied metals are therefore polished on the corners, to avoid artefacts during corrosion tests. They were cleaned using Milli-Q® water, dried with acetone and weighted before testing using a precision balance (accuracy: 0.1 mg).

To reproduce realistic conditions of exposure to water vapour, a calibrated climate chamber is used (Heraeus Vötsch VTRK 300®). This equipment set up is normally used to study corrosion resistance of materials in tropical conditions, where high temperature and water pressure are expected. In the present work, coupons of the metals to be tested are immersed in granular solid salt, in small open vessels. These vessels are then introduced into the chamber at the desired conditions, so that the chamber atmosphere can reach the interface between the salt and the studied metal. Exposure time is 30 days. This experimental setup is sketched on Fig. 1(a), with its main features: heating, cooling and moisture generation.

In addition, temperature and moisture content can be controlled using a thermo-hydrometric probe (Testo® 650) that can be introduced from the side of the chamber. Four testing conditions are studied. At 80 °C, two moisture conditions corresponding to 35 and 24% RH were studied. In these conditions, the salt is respectively in the hexa- and monohydrate state. At 65 °C, two other conditions, 95.6 and 20.1% RH were studied. In that case the salt is respectively dissolved and monohydrate. These conditions give an overview of the different possible conditions, since two points are studied in the monohydrate form, one in the hexahydrate form, and one in accidental conditions (dissolved form), when excessive moisture is introduced into the reactor.

At the end of the test, the samples are removed, ultrasonically cleaned with water and ethanol to remove stuck strontium bromide, dried and visually inspected. Following standards, corrosion products are removed by etching the samples in H_2SO_4 (10 mass %) [51]. Then, cleaning is performed again and the dried samples are weighted. Corrosion rate in µm/month is then estimated, based on the density of the materials.

Some corrosion products were analyzed prior to etching, using X-ray diffraction (XRD) analyses. The XRD was performed with a D500 Bruker X-ray diffractometer with Bragg-Brantano geometry, from 14 to 90° (2θ), using CuKα radiation generated with a voltage of 40 KV and a current of 40 mA. Step size was 0.02° (2θ) with a counting time of 1.2 s. Identification of phases was performed with DiffracPlus software (Bruker) using ICDD database.

To further investigate the corrosion mechanisms, potentiodynamic tests were also performed in a 0.5 M $SrBr_2$ solution using a potentiostat (Amel Instrument, model 2549) at room temperature and 80 °C. In order to match operational conditions, the tests are performed in the presence of CO_2 (Air Liquide). The gas was injected 30 min before the tests and during their whole duration. The open circuit potential (OCP) was first measured. The potential was then varied from OCP to OCP - 800 mV, then from OCP − 800 mV to OCP + 800 mV at a scan rate of 100 mV/min. Potentials are measured using a saturated calomel electrode.

Additional investigations on the corrosion products were made using scanning electron microscope (SEM, FEI®) equipped with EDX (EDAX®).

3. Results

3.1. State of the salt at the testing conditions

Studied conditions are represented on Fig. 1 (b), with the theoretical line of dissolution from Michel et al. [47] and the separation between mono- and hexahydrate, according to Simonova et al. [37]. For the sake of clarity, moisture content is expressed in three different ways: partial pressure of water on the vertical axis and, directly onto the graph, relative humidity (RH) as well as dew point (T_d), which is the control parameter of the climate chamber.

As expected, at (T = 65 °C, T_d = 64 °C), the salt transforms into a thick brine within a few hours. In the other conditions, it remains solid. Nevertheless at (T = 80 °C, T_d = 56.1 °C), the salt is sticky at the end of the test. In the case of copper, the salt takes a turquoise colour in the vicinity of the sample.

3.2. Visual inspection of the metallic samples

All the steel samples exposed to strontium bromide during 30 days have visible spots of corrosion (Fig. 2a–d). In all cases, the observed corrosion can be reattached to the generalised type, and is particularly severe at (T = 80 °C, T_d = 56.1 °C: Fig. 2a), where even the shape of the cylindrical sample is significantly affected. In this case, thick and brittle pieces of rust spontaneously detach from the substrate. In the other cases, a brown powder is dispersed around the sample, contaminating the strontium bromide. After cleaning, some brightness of the substrate is still visible, showing that these products have very little protective effect.

For copper in dissolved salt (T = 65 °C, T_d = 64 °C: Fig. 2g), the surface remains quite uniform and, despite slight tarnishing, it remains

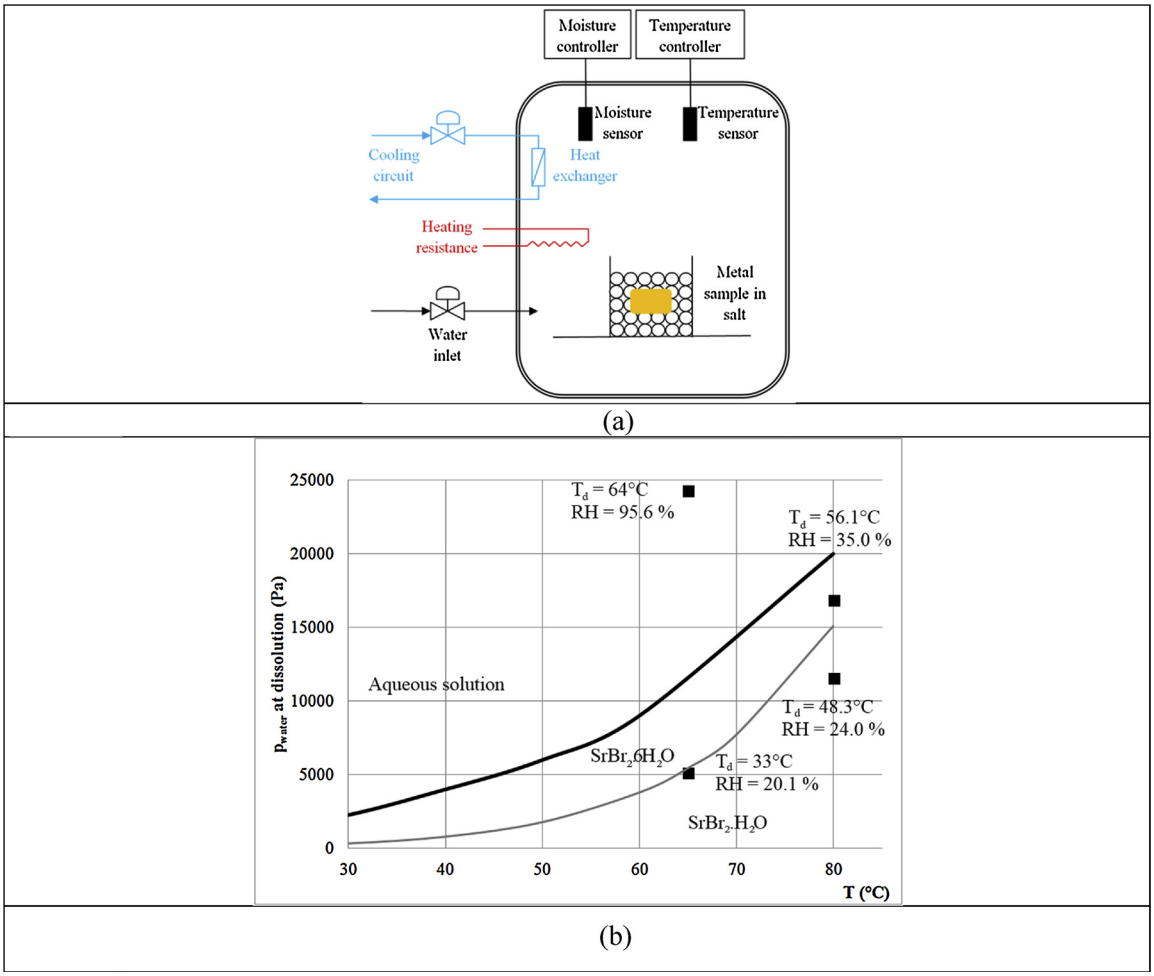

Fig. 1. Tests in the climate chamber device: (a) Experimental setup (b) Testing conditions (dark squares), represented with the expected phases of strontium bromide according to [37,47].

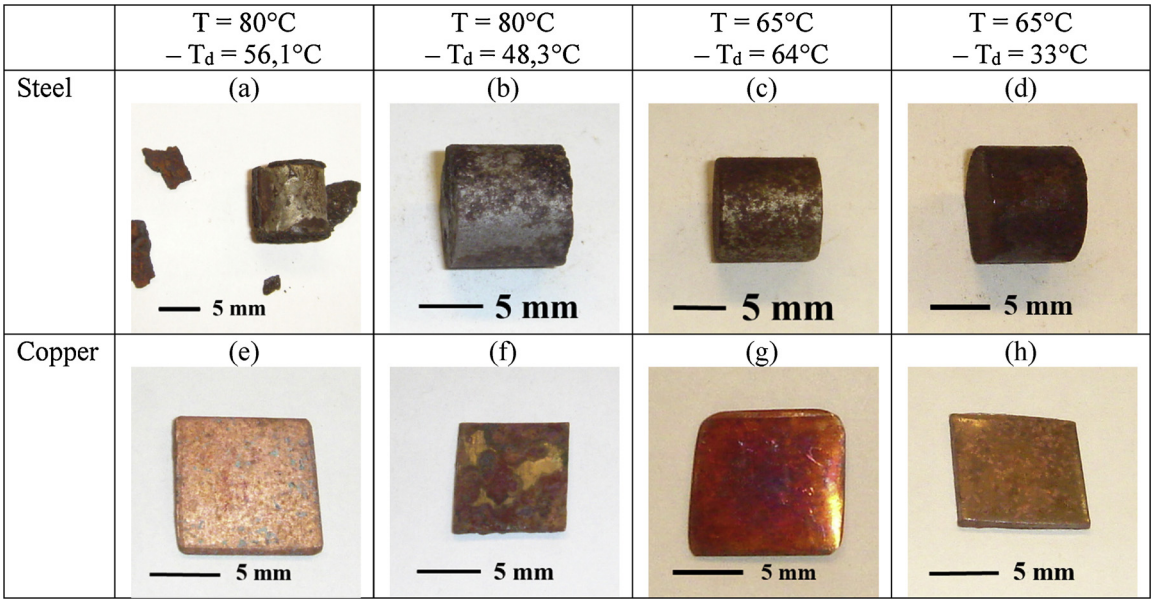

Fig. 2. Samples exposed during 30 days to $SrBr_2$.

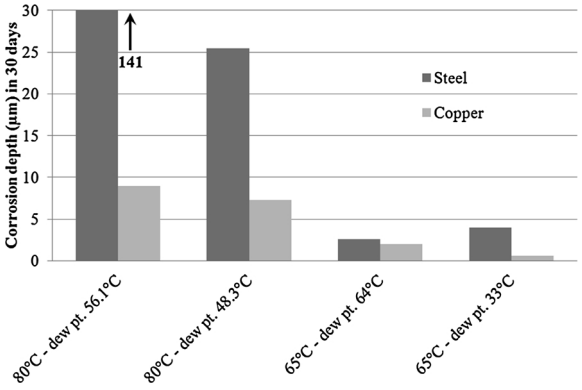

Fig. 3. Corrosion depth of steel and copper in the presence of $SrBr_2$ and moisture (30 days).

quite shiny. In the solid salt, the surface looks more heterogeneous, with some shiny areas and some areas covered by crust, suggesting a different type of interaction with the salt. At (T = 80 °C, T_d = 56.1 °C: Fig. 2e), some turquoise products are visible, while at (T = 80 °C, T_d = 48.3 °C: Fig. 2f), the surface suggests uneven contact with the salt.

3.3. Corrosion rates

Corrosion depths are given in Fig. 3. For all the studied conditions, both materials undergo significant corrosion, but steel is more affected than copper.

Surprisingly, the highest corrosion rate is not necessarily observed when the salt is dissolved: for steel, at 65 °C, worse corrosion is even observed in the solid state (at T = 65 °C and T_d = 33 °C).

Corrosion rate seems very sensitive to temperature: increasing the temperature by 15 °C multiplies the corrosion rate by more than a factor 5 in the monohydrate state.

Another finding is the extremely high corrosion rate observed at 80 °C when the salt is in the hexahydrate form, especially for steel. Care seems needed with simultaneous high temperature and high moisture. Such conditions are expected at the end of the heat releasing phase of the thermochemical reactor, when water vapour pressure is still introduced onto salt that is already delivering heat. Even if 80 °C is not expected as an average output temperature, the reactor is prone to hot spots.

3.4. Corrosion products

In order to obtain indications on the corrosion mechanisms in the most severe conditions, XRD analyses of the studied coupons are given on Fig. 4 and for pure strontium bromide, in order to exclude some overlaps between peaks.

In the case of copper, the peaks of the metallic substrate are clearly visible, which is consistent with the shiny appearance of the copper on Fig. 2. No copper oxide or bromide can be identified on this figure, but several peaks of strontium carbonate are observed. Another diffractogram acquired on the turquoise salt (not presented) shows no carbonate, but strontium bromide and a possible product of reaction between copper and bromine ($Cu_2(OH)_3Br$).

In the case of steel, hematite is the main corrosion product, although magnetite cannot be excluded. At 2θ–25, 36.5 and 44°, peaks of strontium carbonate can be, again, distinguished from the peaks of the other present possible phases. No peak from the substrate could be found, since the analysis was performed on a surface were the corrosion products did not detach.

In both cases, strontium bromide peaks are absent, thanks to the cleaning of the substrate. No such strontium carbonate could be found in strontium bromide that was not contacting the metals, suggesting a role of the metal in its formation.

3.5. Potentiodynamic testing

Fig. 5 a gives the tension-current density relationship of steel at room temperature in 0.5 M $SrBr_2$ solution. At room temperature, the test started at an OCP of -0.63 V vs. saturated calomel. After polarizing the steel at OCP-0.8 V, the curve followed a linear trend around OCP.

OCP corresponds to the following half reaction, according to the Fe Pourbaix diagram:

$$Fe^{2+} + 2e \rightarrow Fe. \quad (1)$$

Fig. 5 b gives the same data at 80 °C. The test started from the OCP, located at −700 mV. After the cathodic excursion, E_{corr} dropped to −800 mV, showing that the solution makes the substrate less noble

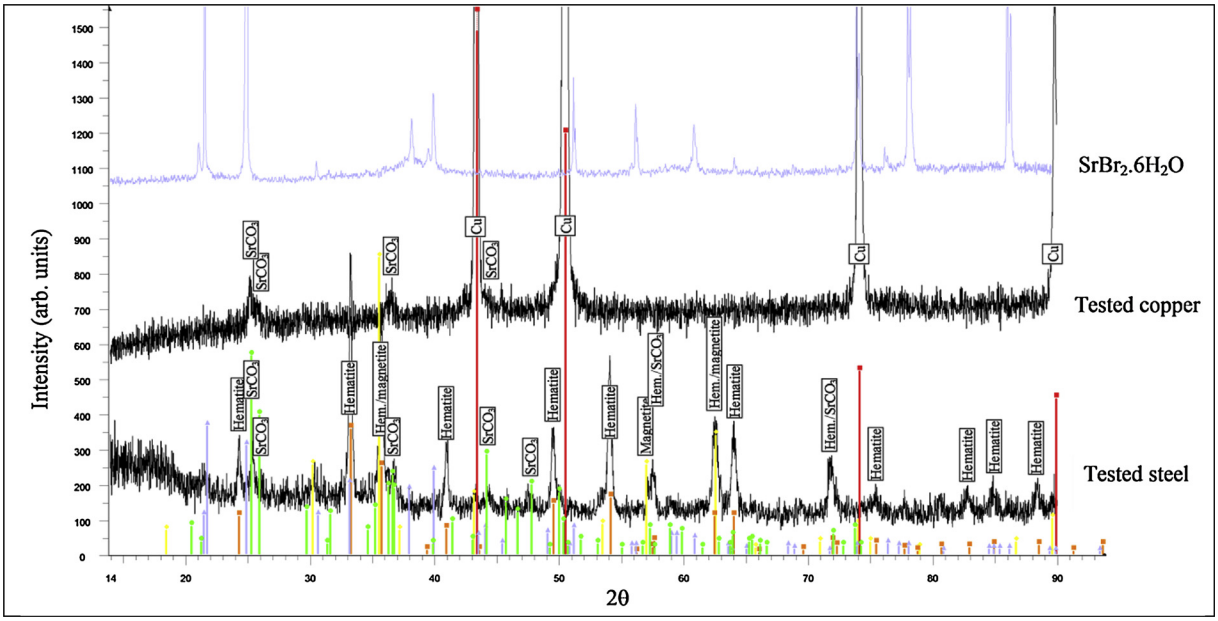

Fig. 4. X-ray diffractogram of corrosion products onto copper and steel, obtained after exposure at (T = 80 °C − T_d = 56.1 °C). Pure strontium bromide diffractogram is provided as well.

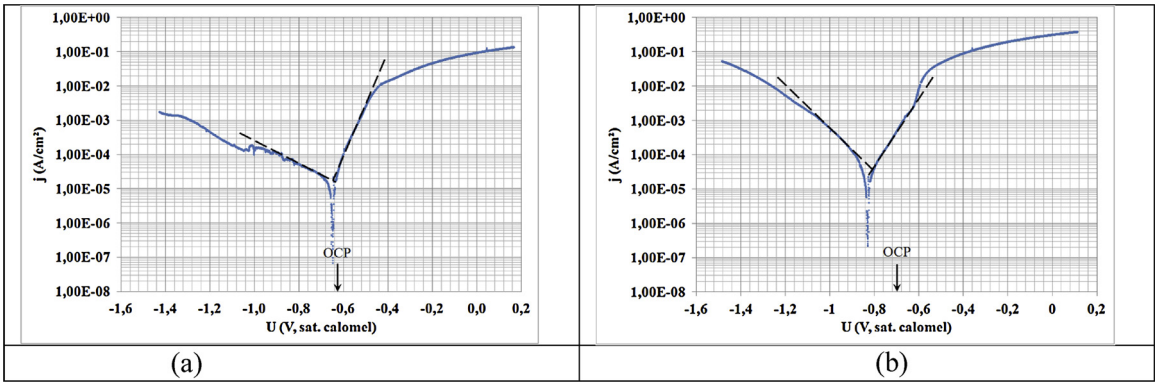

Fig. 5. Tafel plot of ordinary steel (scan from left to right): (a) at room temperature.

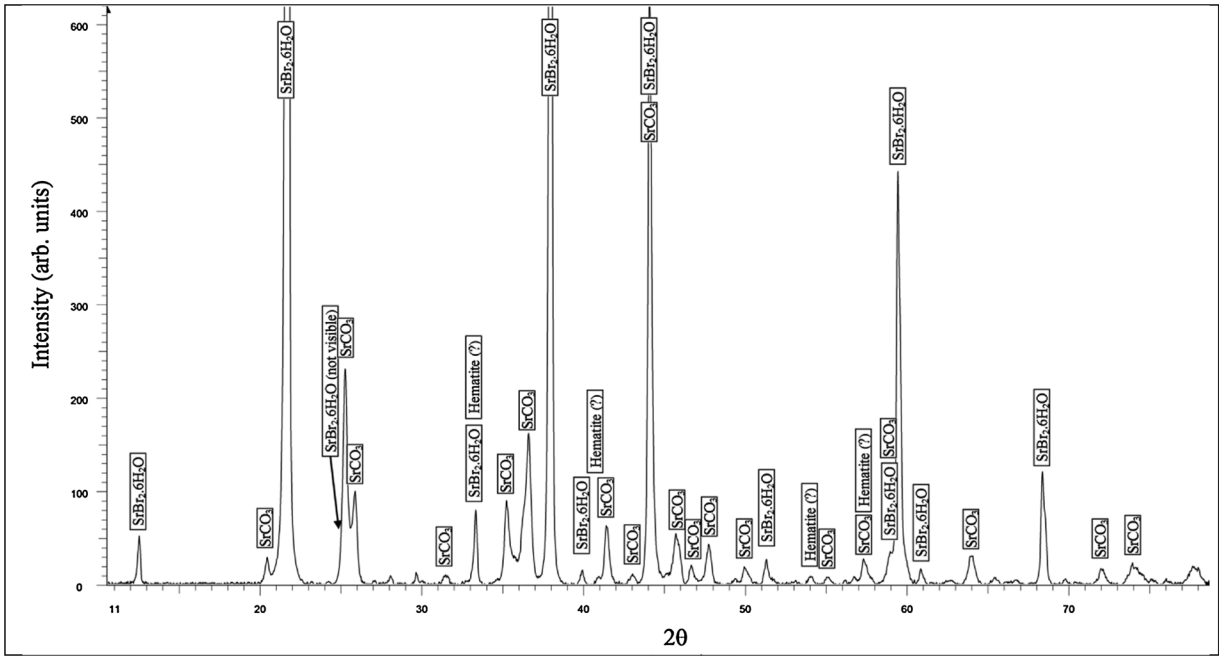

Fig. 6. X-ray diffractogram of corrosion products collected at the bottom of the potentiostat cell after testing steel at 80 °C.

than at room temperature. The solution became more and more opaque due to the formation of brownish products. After the complete cycle, the potential is brought back from the upper potential to OCP. It is noteworthy that after the second reversal, in the anodic excursion, E_{corr} comes back to −700 mV (not shown on the figure). During the experiment, the pH increased from ~3.7 (measured at room temperature, after bubbling CO_2) to ~5.6, compatible with some hydrogen reduction. At 80 °C: it is hard to identify a linear domain on the cathodic side.

The corrosion products (~220 mg) were filtrated and analyzed by XRD: they mostly consist of strontium carbonate, mixed with strontium bromide hexahydrate (Fig. 6). The latter may be due by some evaporation of the solution during filtration. In contrast with Fig. 4, iron oxides are present in small amounts and they can be hardly identified.

Fig. 7 shows micrographs of corrosion products stuck onto the steel surface, after bringing back the electrode to OCP, rinsing and drying. Some of them – a minority – have a characteristic annular shape (Fig. 7a). They are associated with the presence of oxygen and iron and probably correspond to iron oxides or hydroxides. Other precipitates, especially those with a needle shape, massively contain strontium, but the mapping suggests the quasi absence of bromine. The fact that strontium and bromine may be separated is further supported by Fig. 7b, where the EDX spectrum taken on a precipitate ("A" on the figure) shows no bromine, but well developed strontium peak. This finding is consistent with the presence of $SrCO_3$ evidenced by XRD. The remaining of the surface ("B", for instance) mostly consists of iron, that was etched by the test.

Fig. 8 gives the tension-current density relationship of copper at room temperature and 80 °C in 0.5 M $SrBr_2$ solution. Both curves show a similar shape, with a steeper slope on the anodic side, typical of copper. OCP is nearly equal, but currents are higher at 80 °C, suggesting higher kinetics.

Again, it is hard to identify straight lines, here in the cathodic side. In contrast with steel, no degradation product could be filtrated in the flask. Again, the pH increased during the experiment, until ~6. It is believed that copper oxidizes in Cu^{2+} on the anodic side.

Fig. 9 shows the superficial state of copper after bringing back the electrode to OCP. Brittle precipitates are unevenly stuck onto the metal that is locally naked. Additional EDX analysis shows that strontium and bromine appear simultaneously, suggesting the absence of reaction with CO_2.

4. Discussion

The unexpected presence of carbon in the corrosion products during the tests in the climate chamber can be explained firstly, by the carbon contained in the metal itself, secondly, by the carbon dioxide contained

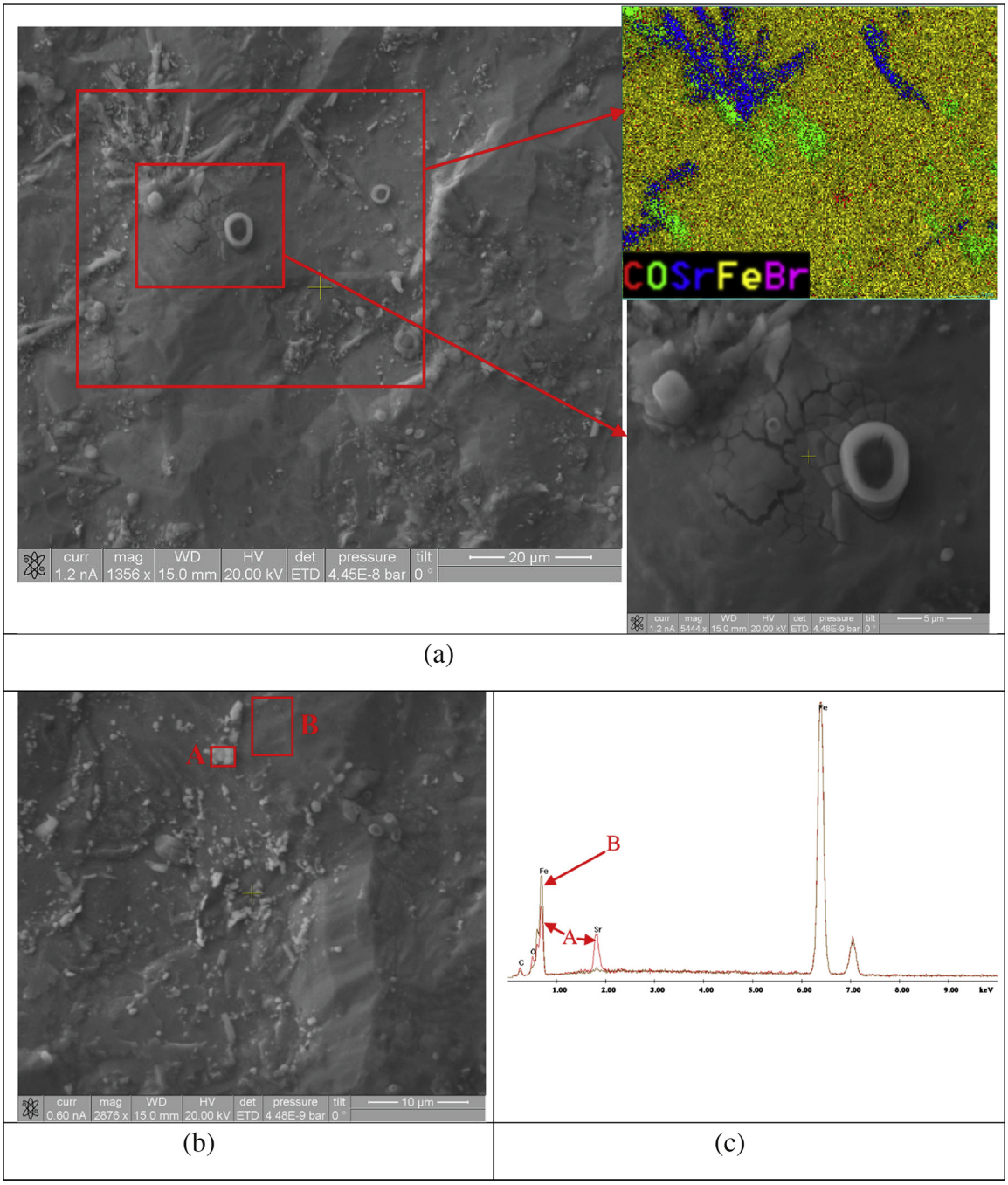

Fig. 7. SEM micrographs and EDX analyses of corroded steel after the polarization test at 80 °C: (a) view showing several types of precipitates, some of them with annular shape.

in the air.

The first explanation cannot be completely excluded in the case of steel, but it does not apply to copper, that is normally poor in carbon.

Regarding the second explanation, no exact data is known for the internal atmosphere of the climate chamber, but the concentration of CO_2 is not likely to be much inferior to 400 ppm, which is the average concentration in the air. Besides, the formation of carbonates in the presence of salts at atmospheric pressure has been demonstrated in several cases yet: CO_2 can react into carbonates either with the metallic substrates or with the cation of the corrosive salt [50,52]. To further sustain this second assumption, the following chemical reaction can be invoked:

$$SrBr_2.\,6H_2O(s) + CO_2(g)(\rightarrow)SrCO_3(s) + 5H_2O(g) + 2HBr(aq.\,,\text{conc.}) \quad (2)$$

Around equilibrium, this degradation of the salt is made possible with sufficiently high partial pressure of CO_2 (in fact, other carbon containing species from the air may play a role), and sufficiently low pressure of water, that is well known in present problem, thanks to the continuous measurement during the tests. The reaction leads to hydrobromic acid in solution of unknown concentration. As a first approximation, data for concentrated HBr will be used. It is likely that the produced water partially acts as a solvent for the acid before being evaporated (indeed, the conditions are such that water is not expected to spontaneously condensate) and that the presence of this solution explains the sticky character of the salt after the test. To verify the

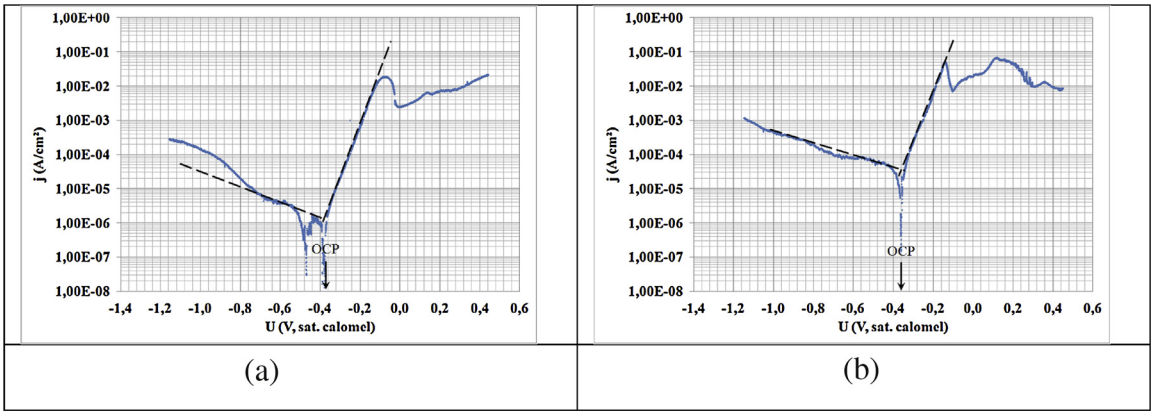

Fig. 8. Tafel plot of copper (scan from left to right): (a) at room temperature.

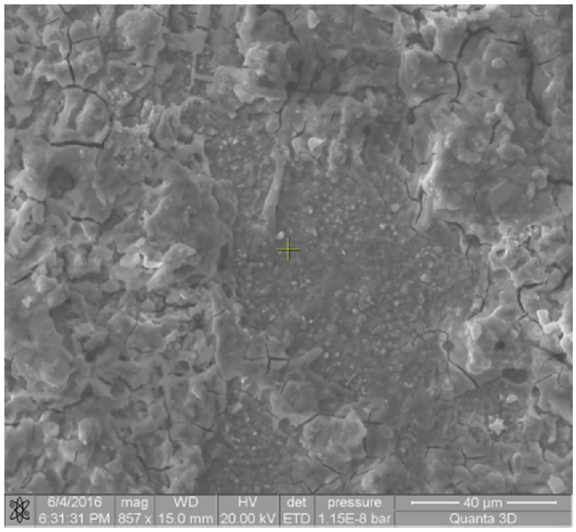

Fig. 9. SEM micrographs of corroded copper after the polarization test at 80 °C.

feasibility of reaction (2), the Gibbs free energy of the reaction ΔG_r is calculated:

$$\Delta G_r = \sum_i \upsilon_i(\Delta H^0_{f,i} - T\Delta S^0_{f,i}) + RT\sum_{gas} \upsilon_{gas} \ln \frac{p_{gas}}{p_{standard}} \quad (3)$$

where υ_i is the stœchiometric coefficient of specie i, $\Delta H^0_{f,i}$ is the standard enthalpy of formation of i at 1 atm and 25 °C), $\Delta S^0_{f,i}$ is the standard entropy of formation and p_{gas} is the partial pressure for each gas involved in the reaction. R is the gas constant. Variations of enthalpy and entropy due to the temperature are neglected, since present system works at relatively low temperature. ΔG_r can now be estimated.

Based on data from Table 1, at a dew point of 56.1 °C, it is shown that reaction (2) is feasible above 35 °C.

These considerations lead to the schematic view of Fig. 10. CO_2 first contacts $SrBr_2.6H_2O$, close to the metallic surface. It produces hydrobromic acid and some water that is progressively pumped by the climate chamber, but that forms a small cell of aqueous solution of HBr first. Strontium carbonate is precipitated. This cell is also likely to directly absorb some additional bromine from the salt. Highly corrosive, it may explain the high corrosion rates that were observed. In the case of steel, it also leads to the observed iron oxides.

Such a mechanism is expected in real life system, where water pressure is also kept constant by mean of a control loop.

At ($T = 65\,°C - T_d = 64\,°C$), the liquid phase totally covers the metallic surface and makes complex the access of air to the surface. This is consistent with the relatively low corrosion rate observed in these conditions and the more even surface of copper.

The potentiodynamic tests only partially reflect these findings. The clear presence of $SrCO_3$ after these tests with steel strongly supports the role of CO_2 in the proposed corrosion mechanism. Nevertheless, this accelerated test suffers from several differences with real life conditions.

The aqueous medium is agitated, due to the continuous injection of CO_2. In contrast, the mechanism suggested by Fig. 10 does not allow evacuating the corrosion products, among them the corrosion products that are very thick, and the hydrobromic acid that is concentrated in a small volume. In the potentiodynamic test, the increase in pH indicates that other factors than HBr production play a role and the acid is diluted.

Also from the thermodynamic point of view, the potentiodynamic test suffers from a lack of representativeness. Several values in Eq. (3) should be modified, because: CO_2 is injected at 1 atm; H_2O is expected to be only in liquid form; the salt is in the aqueous state and there is no equilibrium with solid salt.

Moreover, even if the aim had been solely to study the corrosion by CO_2 the purely aqueous bromide solution, potentiodynamic tests and tension-current density relationship would not have been sufficient to fully identify corrosion mechanisms or to calculate corrosion rates. The presence of different solid coproducts in one case and the non-linearities observed on "Tafel plots" mainly in the second case are observed. This suggests that more than two single oxydo-reduction reactions are needed to describe the corrosion process. The basic assumptions of

Table 1
Data used to verify the feasibility of the reaction (2) at T_d = 56.1 °C.

State	$SrBr_2.6H_2O$ Solid	CO_2 Gas	$SrCO_3$ Solid	H_2O Gas	HBr Aqueous, concentrated
υ	−1	−1	1	5	2
ΔH^0_f(J.mol^{-1})	−2 531 002	−393 500	−1 220 100	−241 800	−120 918
ΔS^0_f(J. mol^{-1}.K^{-1})	175.0	213.8	97.1	188.8	80.7
Reference	[56]	[57]	[57]	[57]	[58]
p_{gas}(Pa)	–	40.52	–	16 800	–

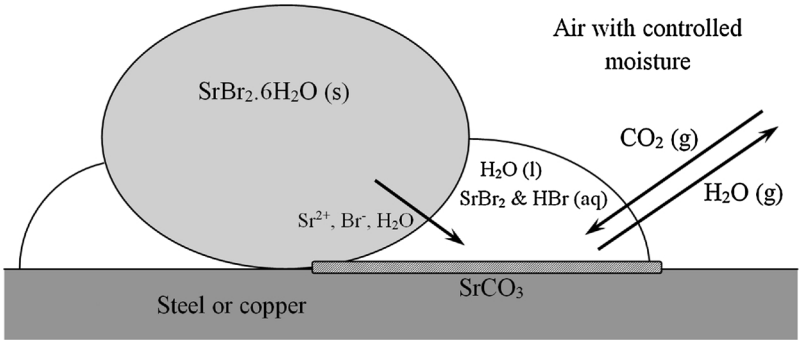

Fig. 10. Schematic representation of the proposed corrosion mechanism at ($T = 80\,^{\circ}C - T_d = 56.1\,^{\circ}C$).

Tafel model are thus not met. These findings corroborate a recent debate on the wrong use of Tafel plots to predict corrosion rates in the presence of CO_2 [53–55]. Impedance spectroscopy measurements might help to better understand the present corrosion mechanism.

From the electrochemical point of view, the nature of the corrosion products gives useful indications on the testing conditions in the climate chamber. No copper oxide or hydroxide is collected in the case of copper, while (non protective) hematite is collected in the case of steel. Based on Pourbaix diagrams, this indicates acidic and strongly oxidizing conditions. These conditions are not properly met by the potentiodynamic test.

5. Conclusion

The proposed testing protocol to assess materials used in thermochemical heat storage reactor reveals significant risks of corrosion. Copper and St37 steel are both severely corroded in contact with $SrBr_2.6H_2O$, especially when the moisture conditions are close to the dissolution of the salt. The fact that the salt remains in a solid or quasi-solid state does not prevent this corrosion phenomenon, with an extrapolated corrosion rate up to above 1 mm per year for steel.

Corrosion rate is strongly dependent on the testing temperature and the partial pressure of water in the testing chamber. However, results show that controlling these parameters is not sufficient to mitigate the problem and that other materials should be proposed.

The particularly high corrosion rate observed at 80 °C, right under the salt dissolution may be explained by the reaction of $SrBr_2.6H_2O$ with atmospheric CO_2, which is supported by the presence of $SrCO_3$ in the corrosion products, leading to corrosive HBr.

Potentiodynamic tests were made in the presence of CO_2, but they revealed strong divergence with real corrosion conditions. In the case of steel, they succeeded to reproduce the formation of $SrCO_3$. Comparing the corrosion products of both tests suggests that real conditions are acidic and strongly oxidizing.

Solutions should be given to mitigate this corrosion problem. A combination of the following strategies is considered for further work:

(i) Changing the material in contact with the salt.
(ii) Encapsulating the salt in an inert matrix, so as to reduce the risk of contact of the salt with metallic surface.
(iii) Designing the thermochemical reactor from the beginning, so as to reduce the occurrence of corrosive conditions (moisture, heat and contact between the salt and a metal).

Acknowledgements

This work was supported by the Walloon Region [grand nr. 6058, SOLAUTARK project]. The authors also acknowledge the "Mecatech" Pole of Excellence, for its confidence in the project.

References

[1] A. Gil, M. Medrano, I. Martorell, A. Lázaro, P. Dolado, B. Zalba, L. Cabeza, State of the art on high temperature thermal energy storage for power generation. Part 1—Concepts, materials and modellization, Renew. Sustain. Energy Rev. 14 (2010) 31–55.
[2] V.M. van Essen, H.A. Zondag, J. Cot Gores, L.P.J. Bleijendaal, M. Bakker, R. Schuitema, W.G.J. van Helden, Z. He, C.C.M. Rindt, Characterization of $MgSO_4$ hydrate for thermochemical seasonal heat storage, J. Sol. Energy Eng. 131 (2009) 0410141–0410147.
[3] A. Fopah Lele, F. Kuznik, H. Rammelberg, T. Schmidt, W. Ruck, Thermal decomposition kinetic of salt hydrates for heat storage systems, Appl. Energy 154 (2015) 447–458.
[4] H. Lahmidi, S. Mauran, V. Goetz, Definition, test and simulation of a thermochemical storage process adapted to solar thermal systems, Sol. Energy 80 (2006) 883–893.
[5] S. Mauran, H. Lahmidi, V. Goetz, Solar heating and cooling by a thermochemical process. First experiments of a prototype storing 60 kW h by a solid/gas reaction, Sol. Energy 82 (2008) 623–636.
[6] B. Michel, N. Mazet, S. Mauran, D. Stitou, J. Xu, Thermochemical process for seasonal storage of solar energy: characterization and modeling of a high density reactive bed, Energy (Oxf., United Kingdom) 47 (2012) 553–563.
[7] M. Molenda, J. Stengler, M. Linder, A. Wörner, Reversible hydration behavior of $CaCl_2$ at high H_2O partial pressures for thermochemical energy storage, Thermochim. Acta 560 (2013) 76–81.
[8] A. Fopah Lele, K. N'Tsoukpoe, T. Osterland, F. Kuznik, W. Ruck, Thermal conductivity measurement of thermochemical storage materials, Appl. Therm. Eng. 89 (2015) 916–926.
[9] L. Jiang, L.W. Wang, R.Z. Wang, Investigation on thermal conductive consolidated composite $CaCl_2$ for adsorption refrigeration, Int. J. Therm. Sci. 81 (2014) 68–75.
[10] O. Myagmarjav, J. Ryu, Y. Kato, Lithium bromide-mediated reaction performance enhancement of a chemical heat-storage material for magnesium oxide/water chemical heat pumps, Appl. Therm. Eng. 63 (2014) 170–176.
[11] A. Solé, C. Barreneche, I. Martorell, L.F. Cabeza, Corrosion evaluation and prevention of reactor materials to contain thermochemical material for thermal energy storage, Appl. Therm. Eng. 94 (2016) 355–363.
[12] K. Ndiaye, S. Ginestet, M. Cyr, Modelling and experimental study of low temperature energy storage reactor using cementitious material, Appl. Therm. Eng. 110 (2017) 601–615.
[13] K. N'Tsoukpoe, T. Schmidt, H. Rammelberg, B. Watts, W. Ruck, A systematic multistep screening of numerous salt hydrates for low temperature thermochemical energy storage, Appl. Energy 124 (2014) 1–16.
[14] Y. Tanashev, A. Krainov, Y. Aristov, Thermal conductivity of composite sorbents "salt in porous matrix" for heat storage and transformation, Appl. Therm. Eng. 61 (2013) 401–407.
[15] E. Courbon, P. D'Ans, A. Permyakova, O. Skrylnyk, N. Steunou, M. Degrez, M. Frère, Further improvement of the synthesis of silica gel and $CaCl_2$ composites: enhancement of energy storage density and stability over cycles for solar heat storage coupled with space heating applications, Sol. Energy 157 (2017) 532–541.
[16] E. Courbon, P. D'Ans, A. Permyakova, O. Skrylnyk, N. Steunou, M. Degrez, M. Frère, A new composite sorbent based on SrBr2 and silica gel for solar energy storage application with high energy storage density and stability, Appl. Energy 190 (2017) 1184–1194.
[17] E. Courbon, M. Frère, N. Heymans and P. D'Ans "Hygroscopic composite material," Patent no. 2015/197788 A1.
[18] S.K. Henninger, S. Ernst, L. Gordeeva, P. Bendix, D. Fröhlich, A. Grekova, L. Bonaccorsi, Y. Aristov, J. Jaenchen, New materials for adsorption heat transformation and storage, Renew. Energy 110 (2017) 59–68.
[19] A. Permyakova, O. Skrylnyk, E. Courbon, M. Affram, S. Wang, U. Lee, A. Valekar, F. Nouar, G. Mouchaham, T. Devic, G.D. Weireld, J. Chang, N. Steunou, M. Frère, C. Serre, Synthesis optimization, shaping, and heat reallocation evaluation of the hydrophilic metal-organic framework MIL-160(Al), ChemSusChem 10 (2017) 1419–1426.
[20] A. Permyakova, S. Wang, E. Courbon, F. Nouar, N. Heymans, P. D'Ans, N. Barrier, P. Billemont, G.D. Weireld, N. Steunou, M. Frère, C. Serre, Design of salt–metal organic framework composites for seasonal heat storage applications, J. Mater.

Chem. A 5 (2017) 12889–12898.
[21] F. Porisini, Salt hydrates used for latent heat storage: corrosion of metals and reliability of thermal performance, Sol. Energy 41 (1988) 193–197.
[22] L. Cabeza, J. Illa, J. Roca, F. Badia, H. Mehling, S. Hiebler, F. Ziegler, Immersion corrosion tests on metal-salt hydrate pairs used for latent heat storage in the 32 to 36 °C temperature range, Mater. Corros. 52 (2001) 140–146.
[23] L. Cabeza, J. Illa, J. Roca, F. Badia, H. Mehling, S. Hiebler, F. Ziegler, Middle term immersion corrosion tests on metal-salt hydrate pairs used for latent heat storage in the 32 to 36 °C temperature range, Mater. Corros. 52 (2001) 748–754.
[24] L. Cabeza, J. Roca, M. Nogués, H. Mehling, S. Hiebler, Immersion corrosion tests on metal-salt hydrate pairs used for latent heat storage in the 48–58 °C temperature range, Mater. Corros. 53 (2002) 902–907.
[25] A. Sarı, K. Kaygusuz, Some fatty acids used for latent heat storage: thermal stability and corrosion of metals with respect to thermal cycling, Renew. Energy 28 (2003) 939–948.
[26] L. Cabeza, J. Roca, M. Nogueés, H. Mehling, S. Hiebler, Long term immersion corrosion tests on metal-PCM pairs used for latent heat storage in the 24 to 29 °C temperature range, Mater. Corros. 56 (2005) 33–38.
[27] A. García-Romero, A. Delgado, A. Urresti, K. Martín, J.M. Sala, Corrosion behaviour of several aluminium alloys in contact with a thermal storage phase change material based on Glauber's salt, Corros. Sci. 51 (2009) 1263–1272.
[28] E. Oró, L. Miró, C. Barreneche, I. Martorell, M. Farid, L. Cabeza, Corrosion of metal and polymer containers for use in PCM cold storage, Appl. Energy 109 (2013) 449–453.
[29] P. Moreno, L. Miró, A. Solé, C. Barreneche, C. Solé, I. Martorell, L. Cabeza, Corrosion of metal and metal alloy containers in contact with phase change materials (PCM) for potential heating and cooling applications, Appl. Energy 125 (2014) 238–245.
[30] G. Ferrer, A. Solé, C. Barreneche, I. Martorell, L. Cabeza, Corrosion of metal containers for use in PCM energy storage, Renew. Energy 76 (2015) 465–469.
[31] F.J. Ruiz-Cabañas, C. Prieto, R. Osuna, V. Madina, A.I. Fernández, L. Cabeza, Corrosion testing device for in-situ corrosion characterization in operational molten salts storage tanks: A516 Gr70 carbon steel performance under molten salts exposure, Sol. Energy Mater. 157 (2016) 383–392.
[32] F.J. Ruiz-Cabañas, C. Prieto, V. Madina, A.I. Fernández, L.F. Cabeza, Materials selection for thermal energy storage systems in parabolic trough collector solar facilities using high chloride content nitrate salts, Sol. Energy Mater. Sol. Cells 163 (2017) 134–147.
[33] F.J. Ruiz-Cabañas, C. Prieto, A. Jové, V. Madina, A.I. Fernández, L.F. Cabeza, Steam-PCM heat exchanger design and materials optimization by using cr-mo alloys, Sol. Energy Mater. Sol. Cells 178 (2018) 249–258.
[34] S. Ushak, P. Marín, Y. Galazutdinova, L.F. Cabeza, M.M. Farid, M. Grágeda, Compatibility of materials for macroencapsulation of inorganic phase change materials: experimental corrosion study, Appl. Therm. Eng. 107 (2016) 410–419.
[35] G.R. Dheep, A. Sreekumar, Investigation on thermal reliability and corrosion characteristics of glutaric acid as an organic phase change material for solar thermal energy storage applications, Appl. Therm. Eng. 129 (2018) 1189–1196.
[36] M.C. Browne, E. Boyd, S.J. McCormack, Investigation of the corrosive properties of phase change materials in contact with metals and plastic, Renew. Energ. 108 (2017) 555–568.
[37] I. Simonova, Y. Aristov, Dehydration of salt hydrate for storage of low temperature heat: selection of promising reactions and nanotailoring of innovative materials, Int. Sci. J. Altern. Energy Ecol. 10 (2007) 65–69.
[38] L. Rigaud, F. Kindbeiter L. Dutruy 2010, "Système thermochimique à enveloppe en matériau composite," Patent no. FR 2 966 572 - A1.
[39] A. Solé, L. Miró, C. Barreneche, I. Martorell, L. Cabeza, Corrosion test of salt hydrates and vessel metals for thermochemical energy storage, Energy Procedia 48 (2014) 431–435.
[40] A. Solé, L. Miró, C. Barreneche, I. Martorell, L. Cabeza, Corrosion of metals and salt hydrates used for thermochemical energy storage, Renew. Energy 75 (2015) 519–523.
[41] M.R. Bloch, A. Bodenheimer, J.A. Epstein, I. Schnerb, Prevention of corrosion of stainless steel by Br_2, Corros. Sci. 11 (1971) 453–461.
[42] J. Leconte, Matériaux pour canalisations de produits chimiques usuels, in: Techniques de l'Ingénieur, (consulted in 2012), Paris, Form. Corr. 670.
[43] G.S. Haines, Materials for bromine containers, Ind. Eng. Chem. 41 (1949) 2792–2797.
[44] ASM International, 9th edition, Metals Handbook vol. 2, ASM International, Metals Park, OH, 1987.
[45] P. Roberge, Handbook of Corrosion Engineering, 2nd ed., McGraw-Hill, New-York, 2012.
[46] Copper Development Association, Corrosion Resistance of Copper and Copper Alloys - CDA Publication No 106, (2016) accessed 10.10.2016 http://copperalliance.org.uk/docs/librariesprovider5/resources/pub-106-corrosion-resistance-of-copper-and-copper-alloys-pdf.pdf.
[47] B. Michel, N. Mazet, S. Mauran, D. Stitou, J. Xu, Thermochemical process for seasonal storage of solar energy: characterization and modeling of a high density reactive bed, Energy 47 (2012) 553–563.
[48] S. Badwe, K.S. Raja, M. Misra, A study of corrosion behavior of Ni-22Cr-13Mo-3W alloy under hygroscopic salt deposits on hot surface, Electrochimica Acta 51 (2006) 5836–5844.
[49] J. Braithwaite, R. Buchheit, Aspects of Two Corrosion Processes Relevant to Military Hardware, Sandia National Laboratories, 1997.
[50] D. Bengtsson Blücher, J.-E. Svensson, L.-G. Johansson, The influence of CO_2, $AlCl_3.6H_2O$, $MgCl_2.6H_2O$, Na_2SO_4 and NaCl on the atmospheric corrosion of aluminum, Corros. Sci. 48 (2006) 1848–1866.
[51] ASTM International, G1-03: Standard Practice for Preparing, Cleaning and Evaluating Corrosion Test Specimens, (2003).
[52] Z.Y. Chen, D. Persson, C. Leygraf, Initial NaCl-particle induced atmospheric corrosion of zinc—Effect of CO_2 and SO_2, Corros. Sci. 50 (2008) 111–123.
[53] A. Kahyarian, B. Brown, S. Nesic, Electrochemistry of CO_2 corrosion of mild steel: effect of CO_2 on iron dissolution reaction, Corros. Sci. 129 (2017) 146–151.
[54] T. das Chagas Almeida, M.C. Bandeira, R.M. Moreira, O.R. Mattos, New insights on the role of CO_2 in the mechanism of carbon steel corrosion, Corros. Sci. 120 (2017) 239–250.
[55] T. das Chagas Almeida, M.C.E. Bandeira, R.M. Moreira, O.R. Mattos, Discussion on "electrochemistry of CO_2 corrosion of mild steel: effect of CO_2 on iron dissolution reaction" by A. Kahyarian, B. Brown, S. Nesic, Corros. Sci. 129 (2017) 146–151, http://dx.doi.org/10.2016/j.corsci.2018.2002.2004 Corrosion Science (in press).
[56] B. Michel, Procédé thermochimique pour le stockage intersaisonnier de l'énergie solaire : modélisation multi-échelles et expérimentation d'un prototype sous air humide, Université Via Domitia, laboratoire PROMES, Perpignan, 2012.
[57] CRC (The Chemical Rubber Co), Handbook of Chemistry and Physics, 92th ed., Taylor&Francis, Boca Raton, Florida, 2011.
[58] CRC (The Chemical Rubber Co), Handbook of Chemistry and Physics, 47th ed., CRC, Cleveland, Ohio, 1966.